ACCURATE REGISTRATION AND FAILURE DETECTION IN TISSUE MICRO ARRAY IMAGES

Musodiq Bello, Ali Can, Xiaodong Tao

Visualization and Computer Vision Lab.
GE Global Research, Niskayuna, NY 12309

ABSTRACT

Image-to-image registration is well-studied, but the challenge of automatically validating registration results remains. In many applications, registration performance is still visually inspected. In Tissue microarrays (TMAs), there are usually hundreds of tissues on a single glass slide, making visual inspection almost impossible. In cases where the TMA slide has to be removed from the microscope and replaced (e.g., in sequential staining, temporal studies, and change analysis), the images on the TMA need to be registered to the corresponding images in the previous steps. The registration has to be robust since undetected registration failure will lead to inaccurate results in subsequent analysis. In this work, we present an automated system to register images of corresponding tissue samples in a TMA, detect registration failures accurately, and automatically re-initialize registration in such cases. The system is image-independent, and reduces the number of cases where the images need to be visually validated. The system has been applied in a study of sequential fluorescent staining of tissue samples on a TMA slide, with 99.88% registration accuracy.

Index Terms— Image registration, Failure detection, Failure recovery, Tissue microarray

1. INTRODUCTION

Recent advances in Tissue Microarray technology (TMA), in which small tissue cores are arranged in a grid on a single glass slide, enable various high throughput gene expression and pathology studies. Due to their numerous advantages, TMA technology (Figure 1(a)) is gradually becoming the standard for multi-patient pathology studies [1]. They allow for high throughput experiments to investigate molecular profiles by immunohistochemistry, immunofluorescence, fluorescent in situ hybridization (FISH), and in situ hybridization [2]. Image registration of tissue samples is a prerequisite in image analysis for TMAs in applications such as sequential staining, temporal analysis, change analysis, expression level, and dose analysis.

A major bottleneck in automated registration systems is the validation which includes the detection and correction of registration failures. This is particularly important because an undetected registration failure will lead to erroneous results in later stages of the automated analysis. The following methods have been used for validating image registration [3, 4]:

i) Visual inspection of combined display of two or more images. This can be done by combining color channels, using two displays with paired cursors, or by using a checkerboard display.

ii) Analysis of image-to-image metric value. This is highly image-dependent, and does not provide information about re-initialization of registration.

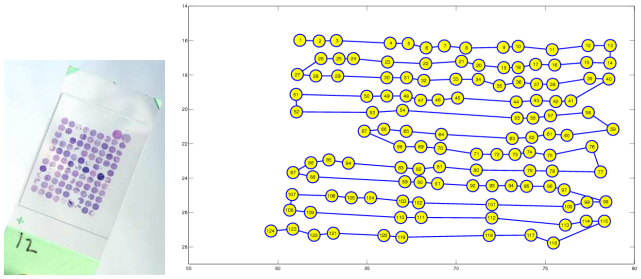

(a) (b)

Fig. 1. (a) A typical TMA slide. (b) Tissue spot diagram of the TMA. The circles represent the tissue spots, and the connecting lines depict the zig-zag pattern of the microscope movement during imaging.

iii) Analysis of resulting transformation. This is useful if there is a ground truth to compare with, e.g., when registering to a synthetic image or an atlas.

iv) Analysis of transformation stability. This can be done by examining the Jacobian of the transform in the neighborhood of the transform returned by the registration method. This approach does not preclude the selection of a local minimum, and does not suggest re-initialization values.

In this work, we present an automated system to register images of corresponding tissue samples in a TMA, detect cases of registration failures with great accuracy, and automatically re-initialize registration in such cases. The system is image-independent (for example, in registering fluorescent and bright-field microscopic images) , and largely reduces the number of cases where the images need to be visually validated. This system is highly valuable in application areas where the TMA slide is moved during image acquisition, thus requiring registration. The system has been employed in a study of sequential fluorescent staining of tissue samples on a TMA slide, with 99.88% registration accuracy.

2. SYSTEMS OVERVIEW

We present a fast, robust, and accurate system to register images of multiple tissue spots, and automatically detect registration failures, which can then be automatically re-registered using newly computed initial parameters. The proposed system is independent of tissue type or image modality. The only requirements are i) the tissue spots must be located on the same slide, and ii) the coordinates of the spots is known. The first condition is always true for tissue spots on a TMA, while the coordinates can easily be obtained from the

imaging microscope for the second condition. The proposed system has seven steps:

1. Images in a small subset are registered initially using default registration parameters in order to establish a ground truth data for exploring the registration parameter space.(Section 4).
2. Registration of all other images with the optimal parameters.
3. Estimation of the global TMA transformation parameters to estimate the misalignment of the TMA slide (Section 5).
4. The estimated global transformation parameters are used to detect images where the registration failed as described in Section 6.
5. All images where the registration failed are re-registered using new initialization values computed from both the global transformation values and the coordinates of each image on the TMA.
6. The re-registered images are assessed for registration failures and cases of failures are identified for user intervention.

The TMA used for validation of the proposed system consists of 177 tissue locations or spots. Each spot has a small sample of breast tissue sectioned at $5\mu m$. The image acquisition protocol consists of sequential rounds of staining with different dyes and bleaching. The image of each TMA spot was automatically captured with a Zeiss AxioImager microscope at 20X magnification, traversing the TMA in a zig-zag pattern. Before any round of staining, an operator places the TMA slide on the microscope, rigidly fixing the top left corner, and calibrates the microscope by recording the relative coordinates of each TMA spot on the microscope. After each round of staining, the operator positions the TMA rigidly as before and makes manual adjustments to obtain a view of the first spot that corresponds to the view obtained in the first imaging round. The microscope then automatically computes the new coordinates of the other spots, relative to the first spot using the coordinates saved in the first round. Our experiments included total of 1612 images from 13 rounds; a sample set is shown in Figure 2.

3. IMAGE REGISTRATION

Registration corrects for global and local transformations. *The global transformation for each staining round is due to positioning the TMA in a different location under the microscope after each round of staining. Local transformation for each image is due to the stage inaccuracy in the microscope system.* The local transformations are in general relatively small compared to the global transformations. It is important to note that registration accuracy is affected mainly by the registration metric, registration parameters, and initialization. Metrics commonly used include mean-squared difference, mutual information, and normalized correlation [5, 6].

The image-to-image transformation is modeled with rigid transformation. Each image i was registered in two image resolution levels to ensure robustness. Matte's Mutual Information metric [7] and a regular-step gradient descent optimizer were used in both levels. In image registration terms, Mutual Information (MI) measures how much information the intensity in one image tells about the intensity in another. Commonly used in multi-modality registration problems [8] due to its robustness, it is well suited for our application where we occasionally have tissue loss and folding. MI is defined in terms of entropy. Given two images A and B, the entropy in the images

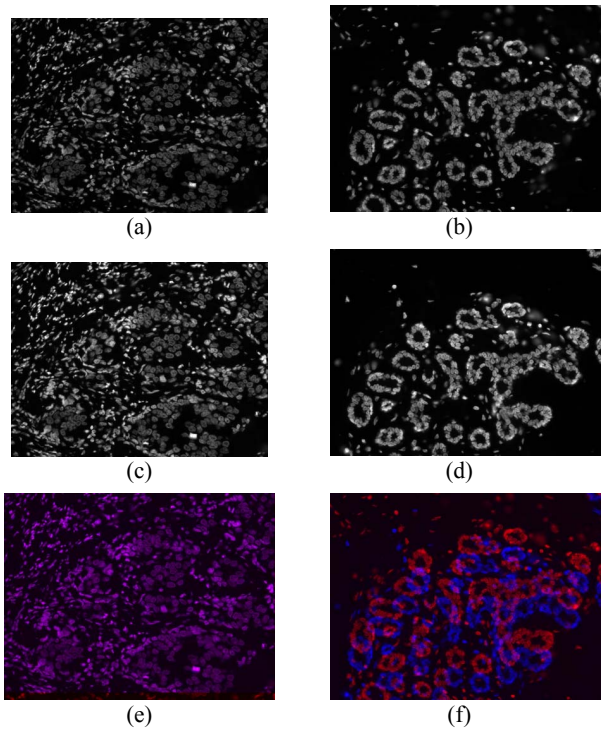

Fig. 2. The images in the first row (a,b) are registered with the images in the second row (c,d). The third row represents both images after registration. The blue represent the reference image, while red represents the transformed image. (e) successful registration, (f) failed registration.

are computed as:

$$H(A) = -\sum p_A(a)\ log\ p_A(a), \tag{1}$$

where $p_A(a)$ denotes the probability that a random pixel in image A has a value a. The joint entropy of the images is represented as

$$H(A,B) = -\sum_A \sum_B p_{AB}(a,b)\ log\ p_{AB}(a,b). \tag{2}$$

The Mutual Information, $MI(A,B)$, between the two images is computed as

$$MI(A,B) = H(A) + H(B) - H(A,B). \tag{3}$$

In MI cost function is optimized using the Mattes et al. [4] method where the user-defined registration parameters include the number of samples and number of bins used to compute the density estimates; the scale parameter that relates rotation to translation; and the optimizer step length.

4. GROUND TRUTH AND TUNING PARAMETERS

We established the ground truth registration only for a subset of one dataset to analyze the sensitivity to parameters and test the performance by running Design of Experiments (DOE). After fixing the parameters we test the performance of the algorithms for the new

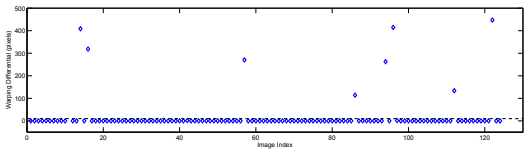

Fig. 3. Distance between the $\mathcal{T}_r$ and $\mathcal{T}_g$ for 124 images. The distance is measured as a warping differential, W. The dashed line (threshold = 10 pixels) separates correct and failed registrations.

datasets by checking the registration failures visually using two-color overlaid images (Figure 2e-f). For the cases where the registration failed, the initialization was manually adjusted and the parameters for the MI metric were manually tuned until the images were correctly registered. The performance of a set of registration parameters is assessed by comparing the resulting transformation parameters with the ground truth transformation values. This comparison is performed by computing the average Euclidean distance between a set of uniformly sampled grid points warped with the ground truth values and the same points warped with the newly computed transformation values.

Let $P = \{P_{(1)}, P_{(2)}, \ldots, P_{(n)}\}$ be a set of n uniformly sampled points in image coordinates. Let $P_g = \{P_{g(1)}, P_{g(2)}, \ldots, P_{g(n)}\}$ be the same set of points after transforming with ground truth transformation $\mathcal{T}_g$, and let $P_r = \{P_{r(1)}, P_{r(2)}, \ldots, P_{r(n)}\}$ represent the points when transformed with another transformation $\mathcal{T}_r$. The warping differential between the two transformations is computed as

$$W_{(g,r)} = \frac{1}{n}\sum_{i=1}^{n}\sqrt{(P_{g(i)} - P_{r(i)})^2}. \tag{4}$$

A threshold is set such that a value of W greater than the threshold indicates a large difference between the two transformations, which in turn implies that the registration represented by the transformation values $\mathcal{T}_r$ is a failure with respect to the ground truth. In our experiments, correct registrations usually have W very close to zero, and a threshold of 10 captures all failed registrations. Figure 3 illustrates the values of W for images in the last staining/bleaching round. The transformations can similarly be compared using distances in the Riemannian space of 2D rigid transforms [9].

After manually establishing the ground truth transformation parameters as discussed in Section 4, we proceeded to find the set of registration parameters that will be optimal for registering all the images. We evaluated different combination of registration parameter values using a full factorial Design of Experiments (DOE). The transformation parameters obtained with each registration was compared with the ground truth parameters by comparing the warping of a regular grid as described in Section 4.

5. REGISTRATION FAILURE DETECTION

Our novel registration failure detection algorithm is based on the fact that all the images are affected by the same global transformation since they are collocated on the same TMA slide. The microscopy stage is calibrated with the images, so that we can easily switch between pixel units in the image coordinate system to metric units in the stage coordinate system.

Registration was performed on individual images in local image coordinate space to obtain parameters of a rigid transformation: the rotation angle θ about the origin (top left corner of image) and two translations in the x and y directions ($\mathbf{t} = [t_x, t_y]^T$). Let the coordinates of a point in an image be $\mathbf{x}_i = [x_i, y_i]^T$ and the coordinates of the same point after registration to the reference (fixed) image be $\mathbf{x}'_i = [x'_i, y'_i]^T$. The registered coordinates $\mathbf{x}'_i$ is related to the original coordinates $\mathbf{x}_i$ as follows:

$$\mathbf{x}'_i = \mathbf{r}_i\mathbf{x}_i + \mathbf{t}_i, \tag{5}$$

where $\mathbf{r} = \begin{pmatrix} \cos\theta & -\sin\theta \\ \sin\theta & \cos\theta \end{pmatrix}$ is the rotation matrix. $\mathbf{x}_i$ and $\mathbf{x}'_i$ are measured in pixels in the local image coordinate system, with the top right corner of the image as origin.

Each transformation is dominated by a global transform introduced during the placement of the TMA at each staining/bleaching round. This implies that there is a global rotation angle Θ and a global translation $\mathbf{T} = [T_x, T_y]^T$ that is common to all the spots on the TMA. Let a point in an image in the TMA coordinate system be $\mathbf{X}_i = [X_i, Y_i]^T$ and the same point after registration be $\mathbf{X}'_i = [X'_i, Y'_i]^T$. $\mathbf{X}_i$ and $\mathbf{X}'_i$ are measured in μm in the TMA coordinate system, with the origin at the top right corner of the first image. If $\mathbf{D}_i$ is the TMA coordinates of the top left corner of the image of tissue sample i on the TMA slide as recorded by the microscope, and p is the pixel size in μm, then the TMA coordinates is related to the local image coordinates by the relations

$$\mathbf{X}_i = p\mathbf{x}_i + \mathbf{D}_i \;\text{ and }\; \mathbf{X}'_i = p\mathbf{x}'_i + \mathbf{D}_i. \tag{6}$$

Note that the coordinates of the first TMA spot which the operator uses to visually align the TMA slide (i.e., the center of TMA rotation) is taken as the origin. The relationship between the original and transformed TMA coordinates is expressed as

$$\mathbf{X}'_i = \mathbf{R}\mathbf{X}_i + \mathbf{T} + \xi_i, \tag{7}$$

where $\mathbf{R} = \begin{pmatrix} \cos\Theta & -\sin\Theta \\ \sin\Theta & \cos\Theta \end{pmatrix}$ is the global rotation matrix and ξ_i is the residual error associated with local transformations from the stage not accounted for by the global transform;

$$\xi_i = \mathbf{X}'_i - \mathbf{R}'\mathbf{X}_i - \mathbf{T}. \tag{8}$$

For all the N images on the TMA, our task is to estimate $\mathbf{R}$ and $\mathbf{T}$ such that ξ_i is minimized. We proceed by computing the mean $\bar{\mathbf{X}}$ and $\bar{\mathbf{X}}'$ for $\mathbf{X}$ and $\mathbf{X}'$ respectively, and compute the correlation matrix. A singular value decomposition (SVD) of the correlation matrix gives a diagonal matrix $\mathbf{D}$ and two unitary matrices $\mathbf{V}$ and $\mathbf{U}$ such that $\mathbf{K} = \mathbf{V}\mathbf{D}\mathbf{U}^T$. The rotation matrix $\mathbf{R}$ is estimated from the SVD as:

$$\hat{\mathbf{R}} = \mathbf{V}\begin{pmatrix} 1 & 0 \\ 0 & det(\mathbf{V}\mathbf{U}^T) \end{pmatrix}\mathbf{U}^T, \tag{9}$$

and the translation estimated as

$$\hat{\mathbf{T}} = \frac{1}{N}\sum_{i=1} N\left(\mathbf{X}'_i - \mathbf{R}\mathbf{X}_i\right) \tag{10}$$

A detailed proof can be found in [10]. The robustness of the algorithm was further improved by using Least Median of Squares [11] estimation method to randomly select a subset of the data to be used for the estimation of the global parameters. This makes the algorithm to be practical even with (theoretically) up to 50% registration failures.

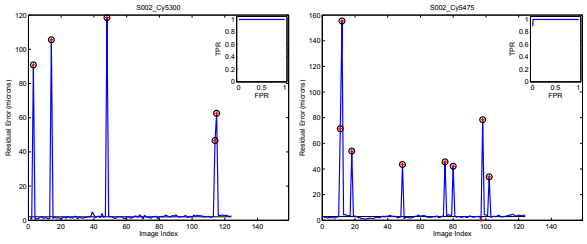

(a) (b)

Fig. 4. Failure detection and ROC curves for two image sets. The blue plots show the residual error of each registration. The median residual error is shown by the straight black line in the bottom. The red crosses are actual registration failures determined by the ground truth comparisons, and the black circles are the registration failures detected by the algorithm using a threshold of $5\mu m$. Inset is the ROC curve obtained by varying the threshold value from 0 to $20\mu m$.

6. RESULTS

The residual error of registration for each image in the TMA is calculated using Equation 8 by substituting the estimated values of $\mathbf{R}$ and $\mathbf{T}$. In our implementation, rather than use a single point to compute residual error, we sampled several points on a grid on the image, taking the average residual error to be the residual error of the image. The median of the residuals for all images in the TMA was then computed. Based on the assumption that most of the images are correctly registered, a failed registration is defined as one where the residual exceeds the median residual value by more than a user-defined threshold value.

To validate the registration failure recovery, we registered the images in our data set using sub-optimal registration parameters that gives about 15% registration failures. The plots of the residual errors for various staining/bleaching rounds are depicted in Figures 4. Varying the threshold values from 0 to $20\mu m$, the receiver operating characteristics (ROC) curves [12] are inset in each plot. The figures show the performance of the proposed algorithms using a threshold value of $5\mu m$. Out of 1,612 images evaluated as described, there was 1 false positive and 3 false negatives. This implies a **sensitivity of 96.6% and a specificity of 99.9%**.

To validate and test the overall system, we again used sub-optimal registration parameters. The registration failure detection algorithm found 85 images to be mis-registered. The initial values for each image was individually computed as shown above, using their coordinates in the TMA. Out of the 85 images, 73 were correctly re-registered in this process, thus leaving only 12 images for manual initialization. This implies that 1,600 images in all were automatically registered using sub-optimal registration parameters; an accuracy of 99.56%.

7. DISCUSSION AND CONCLUSION

In this work, we presented a hierarchical approach to register images of tissue spots on a TMA, and validation results using a sequentially multiplexed protein expression study with 1,612 images. The average execution time is 25 seconds on a standard PC. The optimal registration parameters are learnd using a DOE with small number of samples. This sect of parameters are then applied to all images, resulting in an overall success rate of 99.56%. We also presented a novel algorithm for detecting image registration failures in the TMA. The failed cases are re-initialized for a new round of registration. The method is image-independent, and relies completely on locations of the corresponding images on the TMA to determine when a registration fails. The approach achieves a sensitivity of 96.6% and a specificity of 99.9% for the 1,612 images tested. Given a set of transformation parameters after image registration, it takes about 10 seconds to identify the failures in all the images. We also demonstrated the use of the global parameters obtained to re-initialize the registration, thus boosting registration performance to 99.56%, even with sub-optimal registration parameters.

8. REFERENCES

[1] O. Kallioniemi, U. Wagner, J. Kononen, and G. Sauter, "Tissue microarray technology for high-throughput molecular profiling of cancer," *Human Molecular Genetics*, vol. 10, no. 7, pp. 657–662, 2001.

[2] Francesca Demichelis, Andrea Sboner, Mattia Barbareschi, and Rossana DellAnna, "TMABoost: An integrated system for comprehensive management of tissue microarray data," *IEEE Trans. on Information Technology in Biomedicine*, vol. 10, no. 1, pp. 19–27, 2006.

[3] J. Michael Fitzpatrick, *Detecting failure, Assessing Success*, pp. 117–140, Biomedical Engineering Series. CRC Press, 2001.

[4] L. Ibanez, W. Schroeder, L. Ng, and J. Cates, *The ITK Software Guide*, Kitware, Inc., http://www.itk.org/ItkSoftwareGuide.pdf, second edition, 2005.

[5] Barbara Zitova and Jan Flusser, "Image registration methods: A survey," *Image and Vision Computing*, vol. 21, pp. 977–1000, 2003.

[6] Derek L G Hill, Philipp G Batchelor, Mark Holden, and David J Hawkes, "Medical image registration," *Phys. Med. Biol.*, vol. 46, pp. R1–R45, 2001.

[7] D. Mattes, D. R. Haynor, H. Vesselle, T. K. Lewellen, and W. Eubank, "PET-CT image registration in the chest using free-form deformations," *IEEE Trans. on Medical Imaging*, vol. 22, no. 1, pp. 120–128, January 2003.

[8] J. P. Pluim, J. B. A. Maintz, and M. A. Viergever, "Mutual-information-based registration of medical images: A survey," *IEEE Trans. on Medical Imaging*, vol. 22, no. 8, pp. 986–1004, August 2003.

[9] Vincent Arsigny, Xavier Pennec, and Nicholas Ayache, "Polyrigid and polyaffine transformations: A novel geometrical tool to deal with non-rigid deformations - application to the registration of histological slices," *Medical Image Analysis*, vol. 9, no. 6, pp. 507–523, 2005.

[10] K. Kanatani, "Analysis of 3-D rotation fitting," *IEEE Trans. on Pattern Analysis and Machine Intelligence*, vol. 16, no. 5, pp. 543–549, May 1994.

[11] Thorsten Bernholt, "Computing the least median of squares estimator in time O(nd)," in *Computational Science and Its Applications - ICCSA 2005*, 2005, pp. 697–706.

[12] Tom Fawcett, "An introduction to ROC analysis," *Pattern Recognition Letters*, vol. 27, pp. 861–874, 2006.